

Accepted for publication in The Astrophysical Journal, April 2006 (vol 641)

Multi-Generational Star Formation in L1551

Gerald H. Moriarty-Schieven

National Research Council of Canada, Joint Astronomy Centre, 660 N. A'ohoku Pl., Hilo, HI 96720

g.schieven@jach.hawaii.edu

Doug Johnstone

National Research Council of Canada, Herzberg Institute of Astrophysics, 5071 West Saanich Road, Victoria, BC V9E 2E7, Canada

Department of Physics and Astronomy, University of Victoria, Victoria, BC, V8P 1A1, Canada

doug.johnstone@nrc-crc.gc.ca

John Bally

*Department of Astrophysical and Planetary Sciences,
Center for Astrophysics and Space Astronomy,
Campus Box 389, University of Colorado, Boulder CO 80309*

bally@casa.colorado.edu

and

Tim Jenness

Joint Astronomy Centre, 660 N. A'ohoku Pl., Hilo, HI 96720

t.jenness@jach.hawaii.edu

ABSTRACT

The L1551 molecular cloud, unlike most of the Taurus Molecular Complex, is undergoing a long and sustained period of relatively high efficiency star formation. It contains two small clusters of Class 0 and I protostars, as well as a halo of

more evolved Class II and III YSOs, indicating a current and at least one past burst of star formation. We present here new, sensitive maps of 850 and 450 μm dust emission covering most of the L1551 cloud, new CO J=2-1 data of the molecular cloud, and a new, deep, optical image of [SII] emission (6730Å). We have detected all of the previously known Class 0 and I YSOs in L1551, and no new ones. Compact sub-millimetre emitters are concentrated in two sub-clusters: IRS5 and L1551NE, and the HL Tauri group. Both stellar groups show significant extended emission and outflow/jet activity. A jet, terminating at HH 265 and with a very weak associated molecular outflow, may originate from LkH α 358, or from a binary companion to another member of the HL Tauri group. Several Herbig Haro objects associated with IRS5/NE were clearly detected in the sub-mm, as were faint ridges of emission tracing outflow cavity walls. We confirm a large-scale molecular outflow originating from NE parallel to that from IRS5, and suggest that the “hollow shell” morphology is more likely due to two interacting outflows. The origin of the E-W flow east of HH 102 is undetermined. We confirm the presence of a prestellar core (L1551-MC) of mass 2-3 M_\odot northwest of IRS5. The next generation cluster may be forming in this core. The L1551 cloud appears cometary in morphology, and appears to be illuminated and eroded from the direction of Orion, perhaps explaining the multiple episodes of star formation in this cloud.

The full paper (including figures) can be downloaded at <http://www.jach.hawaii.edu/~gms/l1551/l1551-apj641.pdf>, or viewed at <http://www.jach.hawaii.edu/~gms/l1551/>.

Subject headings: stars:formation; ISM:individual(LDN1551); ISM:jets and outflows; submillimeter

1. Introduction

In stark contrast to most of the Taurus-Auriga star formation complex, which is characterized by very low efficiency formation of isolated stars (Palla & Stahler 2002), the L1551 molecular cloud has sustained a long and continuing period of star formation of relatively high efficiency. The cloud is surrounded by a halo of at least 30 classical and weak T Tauri stars (cTTs, wTTs) and proto-brown dwarfs (Cudworth & Herbig 1979; Jones & Herbig 1979; Feigelson & DeCampli 1981; Feigelson & Kriss 1983; Wood *et al.* 1984; Feigelson *et al.* 1987; Gomez *et al.* 1992; Carkner *et al.* 1996; Briceño, *et al.* 1998; Briceño, Stauffer & Kirkpatrick 2002; Favata *et al.* 2003; Gålfalk *et al.* 2004), indicating star formation activity

over the past few million years. Embedded within the cloud are two known groups of active star formation, one comprised of IRS5 and L1551-NE (hereafter NE), and the other the HL Tau group, located $\sim 5'$ north of IRS5 and consisting of HL Tau, XZ Tau, LkH α 358, and HH 30*. (In the following discussion, HH 30 refers to the Herbig-Haro object(s), while HH 30* (also known as V1213 Tau) refers to the driving star.) The question remains, will this sustained star formation continue beyond the present epoch, and what is the reason for this sustained activity?

LDN 1551 (Lynds 1962), a modest-sized ($M \approx 50 M_\odot$, diameter $D \sim 1$ pc) (Moriarty-Schieven & Snell 1988) dark cloud, lies directly behind the Hyades star cluster in Taurus. Its distance was recently constrained using Hipparchos observations by Bertout, Robichon & Arenou (1999), who determined that the average distance to the Taurus-Auriga complex was 139_{-9}^{+10} pc, but found the distance to T Tauri (which is much nearer to L1551 than the rest of the Tau-Aur complex) to be 168_{-28}^{+12} pc. Extended optical emission from L1551 was first discovered on photographic plates and cataloged as the diffuse [HII] region S239 (Sharpless 1959). This emission was later found to exhibit characteristics of a Herbig-Haro object (shock excited optical emission powered by outflows from young stars) and re-categorized as HH 102 (Strom, Grasdalen, & Strom 1974). Three bright and compact HH objects, HH 28, HH 29, and HH 30, were also found in the region (Herbig 1974). They were at first mis-identified as high velocity stars due to their high proper motions (Luyten 1963, 1971). Recent deep images of the L1551 cloud have led to the discovery of additional Herbig-Haro objects (Graham & Heyer 1990; López *et al.* 1995; Riera *et al.* 1995).

New aspects of the L1551 star forming region continue to be uncovered as deep optical images, high angular resolution radio continuum maps, and other studies are obtained. High angular resolution radio continuum maps have shown that IRS 5, an *FU Ori* type Class I protostar (Sandell & Weintraub 2001), is a binary (Rodríguez *et al.* 1986, 2003a) with a separation of about 50 AU (Looney, Mundy & Welch 1997; Rodríguez *et al.* 1998), total mass $\sim 1.2 M_\odot$, and period ~ 260 yr (Rodríguez *et al.* 2003a). Each star in this system drives a distinct stellar jet (Snell *et al.* 1985; Fridlund & Liseau 1998; Rodríguez *et al.* 2003b) with orientations that are misaligned with the CO outflow lobes, discovered by Snell, Loren & Plambeck (1980), and thought to be powered by IRS 5. Deep optical imaging, proper motion studies, and spectroscopy have provided evidence that the nearby YSO L1551 NE, a Class 0 protostar (Moriarty-Schieven, Butner & Wannier 1995) discovered by Emerson *et al.* (1984), located about $1'$ to the east of IRS 5, may power the bright Herbig-Haro object HH 29 and possibly HH 28 (Devine, Reipurth, & Bally 2000; Hartigan *et al.* 2000) along with a highly collimated 1.5 parsec-long chain of fainter Herbig-Haro objects that are superimposed on the main CO lobes of the L1551 outflow complex. The NE source is also a multiple system (Rodríguez, Anglada & Raga 1995; Moriarty-Schieven *et al.* 2000), and

possesses a molecular outflow (Moriarty-Schieven, Butner & Wannier 1995), although the outflow is aligned with and hence confused by that of IRS5. Associated with IRS5/NE is another low-velocity molecular outflow, the L1551 E-W flow (Moriarty-Schieven & Wannier 1991; Pound & Bally 1991), which extends $\sim 30'$ nearly due west of IRS5/NE, but whose origin is unknown.

Near HL Tauri is a compact group of four or five YSOs, of which all but one have outflows and/or jets (Mundt, Buhrke & Ray 1988). Deep images obtained through narrow-band interference filters transmitting the light of $\text{H}\alpha$ and $[\text{SII}]$ show that the nearby sources HL and XZ Tau and the source of the HH 30 stellar jet power optically visible Herbig-Haro flows which also criss-cross the IRS 5 outflow lobes (Devine, Reipurth, & Bally 1999). Several molecular outflows have also been detected toward this group (Monin, Pudritz & Lazareff 1996).

Most of the surveys for dense cores in the L1551 cloud have concentrated on the IRS5 region (e.g. Moriarty-Schieven *et al.* 1987 for CS, Chandler & Richer 2000 for dust continuum), while Onishi *et al.* (2002) neglected L1551 in their systematic H^{13}CO^+ survey of cores in Taurus. In this work we present 850 μm and 450 μm dust continuum images of a region covering most of the L1551 cloud. In addition, we present new CO $J=2-1$ maps of the cloud, in order to search for new outflows and disentangle those already known.

The full paper (including figures) can be downloaded at
<http://www.jach.hawaii.edu/~gms/l1551/l1551-apj641.pdf>,
or viewed at <http://www.jach.hawaii.edu/~gms/l1551/> .

2. Observations and Data Reduction

2.1. 850/450 μm Continuum Data

850 μm and 450 μm continuum data were obtained using the SCUBA bolometer array (Holland *et al.* 1999) mounted on the James Clerk Maxwell Telescope (JCMT)¹ located near the summit of Mauna Kea, Hawaii. The $20' \times 20'$ region centered on IRS5 was mapped on 12-13 January 2001 using a scan-mapping technique. Sky transparency for these nights was moderately good to good, with $\tau_{225\text{GHz}} \sim 0.06$ on 12 Jan and ~ 0.075 on 13 January.

¹The JCMT is operated by the Royal Observatory Edinburgh on behalf of the Particle Physics and Astronomy Research Council of the United Kingdom, the Netherlands Organization for Scientific Research, and the National Research Council of Canada.

In addition to these data, the SCUBA archive was “mined” for all observations (pointing, calibration, mapping, etc.) taken toward this region between 1997 June and 2002 June (approximately 300 observations in all), and included in the final reduction.

The initial data reduction (switch removal, extinction correction, despiking, etc., but not sky subtraction which was corrected later) were performed using the *oracdr* and *surf* data reduction packages (Jenness et al., 2002). The data were flux calibrated using the archival values derived by Jenness *et al.* (2002). Images were reconstructed using a matrix inversion method described by Johnstone et al. (2000). The reconstructed images are, however, still subject to large-scale “features” which are artifacts of the reconstruction and may not be real. We removed these large-scale structures ($>\sim$ few arcmin) with unsharp masking. The final 850 μm image is shown in Figure 1. The 450 μm image is shown in Figure 2.

Because of archive data mining, some portions of the region, particularly toward HL Tau (which is a SCUBA secondary flux calibrator), have been observed multiple times, and hence the RMS noise of the final image is significantly lower in these locations. In Figure 3 we show a greyscale image of the variance across the image, with contours at 10 mJy beam $^{-1}$ intervals. (Note that the variance towards HL Tau, IRS 5 and NE has been skewed by the brightness of the sources.) In the $\sim 5' \times 5'$ region centered on HL Tau, the RMS is ~ 2 mJy beam $^{-1}$, towards IRS5/NE the RMS is ~ 6 mJy beam $^{-1}$, and throughout much of the rest of the image the variance is ~ 10 mJy beam $^{-1}$. At 450 μm the RMS in the region near HL Tau is ~ 15 mJy beam $^{-1}$, but ~ 70 mJy beam $^{-1}$ through most of the image.

2.2. [SII]

Images were obtained on the nights of December 15, 17, and 19, 2001 with the NOAO MOSAIC2 Camera at the f/3.1 prime focus of the 4 meter Blanco telescope at the Cerro Tololo Interamerican Observatory. The MOSAIC camera is 8192 \times 8192 pixels (consisting of eight 2048 \times 4096 pixel CCD chips) with a pixel scale of 0.26” pixel $^{-1}$ and a field of view 35.4’ on a side. We used a narrow-band filter centered on 6730Å and 6596Å with a FWHM of 80Å for our [SII] and H α observations respectively. Continuum (centered on 7732Å with a FWHM of 1546Å) images were also obtained, but will be presented in another paper.

In order to increase our observing efficiency, we opted not to take a set of five images in the standard MOSDITHER pattern which is normally used to eliminate cosmic rays and the gaps between the individual chips in the MOSAIC camera. Instead, we took a single image in each filter for each pointing. As a result of this observing strategy, most of our images still contain chip gaps, resulting in a loss of approximately 3% of the area coverage at each

pointing. However, using this strategy, we were able to effectively cover a 7.5 square degree area in our allotted three nights.

Images were overscanned, trimmed, bias subtracted, and flat fielded (using dome flats) in the standard manner using the MSCRED package in IRAF. Cosmic rays were removed using CRNEBULA². Because we used single exposures in much of the survey, the images may contain a small number of cosmic rays which were not eliminated by the CRNEBULA task, however we can safely distinguish the cosmic rays from objects by their morphology: cosmic rays have sharp edges and are often only one pixel in extent.

We used the procedures MSCCMATCH, MSCIMAGE, and MSCIMATCH to remove relative distortions, generate a single extension FITS image, and match the sky background between images. For the pointings for which we obtained multiple images in each filter in a dither pattern, we used the MSCSTACK procedure to combine all images in each filter into a single image which eliminates the gaps between CCD chips.

A portion of the [SII] image, covering the L1551 cloud, is shown in Figure 4.

2.3. CO $J = 2 - 1$ Emission

CO J=2-1 observations were obtained at the (former) National Radio Astronomy Observatory (NRAO) 12 meter diameter Cassegrain radio telescope located on Kitt Peak Arizona in January and February of 1997. The telescope has a pointing accuracy of 5", an aperture efficiency of 32%, and main beam efficiency of 44% at 230 GHz. At 230 GHz, the beamsize is 27". The 200 to 265 GHz SIS receiver had a single-sideband receiver noise temperature of about 200 K providing a system temperature around 500 K. This dual channel receiver acquires data in two orthogonal polarization states simultaneously. The system back-end consisted of a 768 channel hybrid spectrometer with each channel delivering a bandwidth of 195.3 kHz for a total bandwidth of about 150 MHz. At 230 GHz this corresponds to 0.25 km s⁻¹ per channel and an overall bandwidth of 192 km s⁻¹.

Spectra were acquired using on-the-fly (OTF) mapping, wherein the telescope is rastered rapidly across the sky while data and antenna position information are recorded at a 10 Hz rate (Mangum 1997). The telescope was rastered across 30' rows. After each row, the

²The CRNEBULA task removes cosmic rays from a region with fine nebular structure which can be misidentified by more traditional cosmic ray rejection routines. The routine uses box and ring median filters to distinguish fine nebular structure from cosmic rays. For a detailed discussion of how this procedure works, see the IRAF CRNEBULA help page (available at <http://iraf.noao.edu/scripts/irafhelp?crnebula>).

telescope was moved $6.9''$ perpendicular to the row and scanned in the opposite direction. Following the completion of each pair of rows, the telescope was position switched to an emission-free reference position and a calibration observation (ambient temperature load and sky emission) was obtained. The reference position was located at $\alpha(2000) = 4^h32^m57^s.87$, $\delta(2000) = 17^\circ52'58''$, which was found to be emission-free to 0.1 K at all velocities. The telescope pointing was checked several times during each observing session and the carbon star IRC+10216 was used as an absolute intensity calibration source.

The telescope raster orientation was chosen to be either aligned with or orthogonal to a position angle of 60° which is close to the orientation of the IRS 5 outflow. Each field was observed many times with alternating orthogonal raster orientations. The resulting map covers a $30'$ by $52'$ field with a major axis tilted at $PA = 60^\circ$. There are substantial horizontal and vertical stripes in the raw images along the principle directions of the OTF scanning (at $PA = 60^\circ$ and $PA = 150^\circ$). This artifact is produced by high order baseline ripples and calibration differences between receivers. The striping was partially eliminated by cross-calibration of orthogonal scans ('basket weaving') and by fitting higher order baselines to the data.

The entire data set was reduced using the AIPS data reduction package. The reduced spectra were re-sampled onto a uniform $10''$ grid and first-order baselines were subtracted. The resulting rms noise per 195.3 kHz channel is about 0.1 K at each grid point. All further reductions and analyses were conducted with the IDL and COMB data analysis packages.

Channel maps of the CO data are shown in Figure 5.

3. Results

The dust continuum image shown in Figure 1 clearly shows three distinct regions of emission. In Figure 6 these regions are identified with optical features, i.e. toward the HL Tau group, associated with IRS5 and NE and their outflows, and toward a dark ridge or core extending north-west of IRS5.

All known Class 0/I YSOs (IRS5/NE/HL Tau) were detected. Two cTTs (Class II) (XZ Tau/LkH α 358) were detected near HL Tau where the RMS of the image is especially low. No other cTTs or wTTs (Class II/III) were detected at the RMS of the image. No previously unknown stellar objects were detected. We have detected one starless core, in which Swift, Welch & Di Francesco (2005) have found evidence for collapse.

The flux densities and integrated intensities of the detected sources and regions are

tabulated in Table 1. These, as well as deconvolved source sizes (from gaussian fits), were determined using IDL routines. Background emission was subtracted from all of the compact or slightly resolved sources, while the derived flux densities of the extended sources have had internal “point” sources already subtracted. Care should be taken, however, in interpreting the results of these extended structures, since the maps were made by chopping on the sky, and the image reconstruction method has difficulty restoring large-scale structure (Johnstone *et al.* 2000).

The mass of each source/region, shown in Table 1, was derived by assuming a dust temperature of 20 K and an opacity law with $\kappa_{850} = 0.02 \text{ cm}^2 \text{ g}^{-1}$ at 850 μm (implicit in this is the assumption of a gas to dust mass ratio of 100). At a distance of 168 pc (Bertout, Robichon & Arenou 1999) the integrated flux (S_{850}) to mass ratio is

$$M_{\text{clump}} = 0.14 * \left(\frac{[\exp(17/T_d) - 1]}{[\exp(17/20) - 1]} \right) \left(\frac{\kappa_{850}}{0.02 \text{ cm}^2 \text{ g}^{-1}} \right)^{-1} \left(\frac{D_{L1551}}{(168 \text{ pc})} \right)^2 S_{850} \text{ M}_\odot.$$

We shall discuss each region separately.

3.1. HL Tau Group

Figure 7 shows a close-up of the HL Tau region in [SII] with 850 μm contours superimposed. The [SII] image shows the jets associated with HL Tau, HH 30* and XZ Tau. HL Tau, a Class I protostar, is by far the brightest source in this region, with peak intensity 2.2 and 9.6 Jy beam $^{-1}$ at 850 and 450 μm respectively (Table 1). HL Tau may have been barely resolved ($\sim 6''$ at 850 μm , $\sim 4.5''$ at 450 μm , fitted using IDL routines).

The deeply extinguished edge-on disk source HH 30* was also clearly detected at 0.05 Jy beam $^{-1}$ (Table 1). At 450 μm (Figure 2) it can be seen, but is difficult to extract from the extended (plateau) emission. The HH 30 jet does not seem to have any related dust continuum emission. LkH α 358 and XZ Tau, two Class II sources, were less clearly detected because of their proximity to HL Tau, but create significant “deviation” in the 850 and 450 μm contours (Figures 7 & 8) around HL Tau.

Although we have clearly detected HL/XZ Tau, LkH α 358 and HH 30*, we do not see any evidence for a source VLA1-HL Tau (Brown, Drake & Mundt 1985), located $\sim 12''$ east-north-east of HL Tau (see Fig. 8) and proposed to be the origin of a jet in the vicinity of HL Tau (Mundt, Brugel & Buhrke 1987; Mundt, Buhrke & Ray 1988). This source has also not been detected at any other wavelength, placing further doubt that VLA1 is a young stellar object or protostar.

Surrounding the stellar group is a broad ($\sim 2.5' \times 4'$), “plateau” of emission, with typical

intensity $\sim 0.03\text{--}0.06$ Jy beam $^{-1}$ and integrated intensity ~ 5 Jy after subtracting the point sources (above). This extended emission may be of concern for JCMT calibration, since HL Tau is one of the secondary flux calibrators for SCUBA.

The HL Tau jet at position angle $PA \sim 51^\circ$ (Mundt *et al.* 1990; López *et al.* 1995) may drive HH 266 located northeast of these stars (e.g. Figures 1 & 2 in Devine, Reipurth, & Bally 1999). A $48''$ long blueshifted jet with a heliocentric radial velocity (v_{hel}) = -180 km s $^{-1}$ extends to the northeast and a $65''$ long redshifted jet with $v_{hel} = +120$ km s $^{-1}$ extends to the southwest.

An optical outflow originating from XZ Tau can be traced more than $1'$ at $PA \sim 15^\circ$ from this binary star. This flow is blueshifted with $v_{hel} = -45$ km s $^{-1}$ towards the northeast and redshifted with $v_{hel} = +77$ km s $^{-1}$ toward the southwest (see Krist *et al.* 1999 for HST images).

The HH 30* jet at $PA \sim 31^\circ$ lies within a couple degrees of the plane of the sky (Mundt *et al.* 1990; López *et al.* 1995). Mundt et al. (1990) traced this jet for $135''$ towards the northeast and $85''$ towards the southwest with a heliocentric velocity of $v_{rad} = +16$ km s $^{-1}$ towards both lobes. On deep H α and [SII] images, HH 30* can be traced to the main L1551 outflow lobe and possibly beyond. Thus, this outflow may influence the HH complex located SW of IRS 5.

At velocities between 8 km s $^{-1}$ and 14 km s $^{-1}$ (Figure 5) an arc of molecular gas extends from the IRS 5 region towards the north. Lower resolution maps in $^{12}\text{CO}_{1-0}$ and $^{13}\text{CO}_{1-0}$ led to the suggestion that this feature is related to the HH 30* outflow (Pound & Bally 1991), but the $^{12}\text{CO}_{2-1}$ maps indicate that this feature lies east of HH 30*. It may, however, be related to one of the flows emerging from the HL-Tau complex.

The jet trajectories, overlaid on the $^{12}\text{CO}_{2-1}$ emission from $v_{LSR} = 2$ km s $^{-1}$ to 6 km s $^{-1}$ and from $v_{LSR} = 9$ km s $^{-1}$ to 14 km s $^{-1}$ are shown in Figure 9. The blue-shifted CO emission near HL and XZ Tau forms a shell-like frame around the axes of the HL and XZ Tau jets. The CO has a projected angular extent of about $5'$ or 0.2 pc and can be traced from $v_{LSR} = 0.5$ km s $^{-1}$ to 6.5 km s $^{-1}$ where the lobe is lost in the ambient cloud. There is no apparent red-shifted emission associated with the southward jets, although a finger of red-shifted emission may be tracing the northward jet of HH 30*, which is nearly in the plane of the sky.

3.2. L1551-IRS5/NE

Figure 10 shows an optical [SII] image of the region near IRS5/NE and toward the southwest outflow lobe, with $850\mu\text{m}$ dust emission contours superposed. Figure 11 is a similar figure toward the north-east of NE. IRS5 is located at the apex of an optical jet, while NE is not seen at all optically. NE has been classified as a Class 0 source (Moriarty-Schieven, Butner & Wannier 1995) and IRS5 a Class I FU Ori protostar (Sandell & Weintraub 2001).

IRS5 is the brightest submillimeter source in the Taurus complex, with peak intensity $3.16 \text{ Jy beam}^{-1}$. NE has a peak intensity of $1.16 \text{ Jy beam}^{-1}$ (Table 1). Both are extended ($\sim 10''$), with large envelopes, that join with a ridge of emission (Plateau in Table 1).

Three known molecular outflows originate from this region, the IRS5 flow, the NE flow, and the L1551 E-W flow. Optical imaging (e.g. Devine, Reipurth, & Bally 1999) indicates that some of these flows may in turn be powered by several distinct sources.

The main IRS5 flow is oriented northeast-southwest, is associated with HH 28, 29, 102, 258, 259, 262 & 286, and may be driven collectively by the IRS 5 binary and L1551 NE. The recently recognized *L1551 NE Flow* associated with HH 454 has the same orientation and is confused with the main L1551 flow. The *E-W flow* consists of a $25'$ long redshifted east-west oriented CO ridge extending from HH 102 in the IRS 5 region towards the west.

We look at each outflow in turn.

3.2.1. The Main L1551 Flow

Figure 12 shows the main L1551 outflow along with the mean of the orientations of the two IRS 5 jets (Fridlund & Liseau 1998) at $PA = 246^\circ$. The projected extent of the outflow is about 0.45° or about 1 pc. The southwest lobe is blueshifted while the northeast lobe is redshifted with respect to the ambient cloud (centered at $v_{LSR} = 6.75 \text{ km s}^{-1}$). The southwest lobe extends from -7 km s^{-1} to $\sim 8.6 \text{ km s}^{-1}$ and consists of a hollowed out half-shell at low velocities that narrows at high v_{LSR} . The northeast lobe extends from $v_{LSR} = 4.5 \text{ km s}^{-1}$ to 22 km s^{-1} and is considerably smaller than the southwest lobe; it contains three connected clumps that surround a low-emission region with the clump furthest from IRS 5 coinciding with HH 262. Unlike the southwest lobe, the northeast lobe appears closed both spatially and kinematically. Figure 13 shows a velocity slice along a line connecting HH 262, IRS 5, and HH 28. Multiple peaks of emission, both blueshifted and redshifted, provide evidence that both the southwest and northeast lobes have been affected by multiple outbursts from a single source, or by separate outflows from different sources.

It is important to point out that we detected several HH objects associated with the IRS5/NE main outflow complex well beyond the projected edge of the L1551 cloud (e.g. HH 286; Devine, Reipurth, Bally 1999). HH 286 is a large but dim H α bow shock 20' northeast of IRS5. Many galaxies are seen in this portion of the Mosaic images. The CO lobes only extend as far as the projected edge of the CO cloud. The outflow, however, continues on and produces shocks in either neutral or ionized gas. These shocks are seen as these HH objects beyond the projected edge of the cloud.

In Figure 14 we plot contours of 850 μ m emission on top of a grey-scale images of CO emission (10-12 and 4-6 km s $^{-1}$). In Figure 14 (above) we see a ridge of weak 850 μ m emission tracing the north limb of the blue-shifted outflow from IRS5 out to HH 102. This ridge can be seen more clearly in Figure 10. HH 102 is also clearly detected at 850 μ m, coincident with the optical emission (Figure 10 but offset to the west of the CO intensity peak (Figure 14). From the south edge of HH 102, a finger of 850 μ m emission extends eastward back toward IRS5, perhaps indicating a bow shock. In addition, faint extended emission can be seen in Figure 14 toward the peak of the CO emission in the south limb of the IRS5 southeast lobe.

The continuum emission measured by SCUBA may be contaminated by strong molecular line emission within the passband (Johnstone *et al.* 2003). Such conditions are most likely to occur for strong lines, such as ^{12}CO 3-2, in environments with broad kinematic features such as shocks and jets. We have analyzed the relatively few available ^{12}CO 3-2 spectra taken with the JCMT and determine that the typical integrated line strength in the outflow lobes is \sim 30 K km s $^{-1}$. This agrees well with the mapped ^{12}CO 2-1 observations presented in this paper. About one third of the integrated line strength is due to the underlying molecular cloud and varies only slightly across the region. This emission is chopped out of the SCUBA observations. The remaining \sim 20 K km s $^{-1}$ is highly variable on scales of less than two arcminutes and may contribute to the observed SCUBA flux. At this strength, the CO contamination is estimated to produce \sim 15 mJy beam $^{-1}$ of contaminated emission, compared with the typical 100 mJy beam $^{-1}$ measurement in the main L1551 lobe. Thus, contamination, while not negligible, is not the main source of the observed SCUBA emission, except possibly in the very weak continuum emission joining IRS5 and HH 102, and toward the south limb of the southwest lobe. The continuum emission, therefore, most likely comes from swept up dust around the outflow lobe.

3.2.2. The L1551 NE Flow

Deep narrow-band images and proper motion measurements of HH 29 show that it is likely to be powered by a bipolar HH flow from L1551 NE and *not* IRS 5 as had previously

been thought (Devine *et al.* 2000). HH 29 lies within a few degrees of the axis of a blueshifted jet visible in the $1.644\text{ }\mu\text{m}$ line of [Fe II] that originates from L1551 NE and points towards the bow shock HH 29. A chain of compact [SII] emitting HH objects, HH 454, lie along the axis of this jet (Figure 12; Devine, Reipurth, & Bally 1999). Extending this jet axis through HH 454a (which can be seen in Figure 11 as a compact knot of [SII] emission adjacent to NE to the south-west) intersects HH 28 and HH 29. Extending the axis to the north-east intersects HH 454b/454c (seen in Figure 11 as slightly more diffuse knots $\sim 0.7'$ and $\sim 1'$ from NE) and the weak bow shock of HH 262E at $04^h32^m10^s +18^\circ12'15''$.

In Figure 11, HH 262 has clearly been detected at $850\text{ }\mu\text{m}$. In addition, a weak ridge of emission appears to connect the north rim of HH 262 with NE, similar to the ridge of emission connecting HH 102 to IRS5. This emission, however, is of order 70 mJy beam^{-1} ; though contamination due to CO emission may be significant at this intensity, there is little apparent CO emission at this location (Figure 14).

Given the roughly parallel jets from IRS5 and NE, it is likely that the outflows from these sources are interacting with each other. Moriarty-Schieven, Butner & Wannier (1995) first detected the NE outflow, but because of limited mapping and confusion with the IRS5 outflow they concluded that the blue-shifted outflow lobe was oriented to the northeast, i.e. toward HH 262. In Figure 14 (lower), however, the northeast lobe red-shifted emission peaks at NE, and appears as a limb-brightened ellipse with one end at NE, suggesting a significant amount of the red-shifted outflow originates from NE. The blue-shifted emission within the northeast lobe (Figure 14 upper) appears disconnected from NE, and may be from the near side of the outflow cavity. There is significant blue-shifted emission peaking at NE, but extending toward the southwest, as suggested by the fan-shaped reflection nebula in this direction (Graham & Heyer 1990). This suggests that the NE outflow is mostly parallel to that from IRS5. Indeed, Devine, Reipurth & Bally (1999) have proposed that HH 29 is driven by NE based on proper-motion studies, and note that a nearly straight line can be drawn connecting NE and HH 29 with HH 28, HH 262, and HH 286.

Devine, Reipurth & Bally (1999) were uncertain whether NE or IRS5 were the originating source of HH 262 based on their proper-motion studies, although the orientation was suggestive. Lopez *et al* (1998), also using proper motion and kinematic studies, concluded that the proper motion of this source was “roughly” away from IRS5. They dismissed the possibility that NE was the origin, however, only because Moriarty-Schieven, Butner & Wannier (1995) assumed the NE blue lobe were oriented to the north-east toward HH 262, whereas the kinematics of the HH object were red-shifted. Our new CO data confirm that the outflow orientation is the correct direction for NE to be the origin of HH 262E, and, by extension, HH 286. With HH 29 and possibly HH 28 and HH 259 originating from NE, the

south limb of the blue-shifted outflow lobe may also originate from NE. The “hollow shell” morphology proposed for this outflow (Snell, Loren & Plambeck 1980; Moriarty-Schieven *et al.* 1987, 1988), may instead be due to two interacting outflows.

3.2.3. The E–W Outflow

A third outflow originates from the region containing IRS5 and L1551NE that extends due west from the L1551 cloud core (Figure 5, $8\text{--}12\text{ km s}^{-1}$). This feature, called the E–W flow (Moriarty-Schieven & Wannier 1991; Pound & Bally 1991), is a $30'$ (1.0 pc) long finger of redshifted gas at PA = 270° extending from near IRS 5 toward the west with a maximum width of 0.1 pc. The E–W flow has a relatively small velocity extent ranging from about 6.5 km s^{-1} to 11.0 km s^{-1} and has no obvious blueshifted counterpart. NE was originally proposed as the origin for this outflow, but we see that this source powers an outflow parallel to that from IRS5. However, L1551 NE may be a multiple star system (Rodriguez, Anglada, & Raga 1995; Moriarty-Schieven *et al.* 2000) and the companion star may be a viable candidate to drive the E–W flow.

The new CO data shows that the eastern end of the E–W outflow lobe coincides with the northwestern rim of the main L1551 outflow shell and the Herbig-Haro object HH 102. The lobe consists of a pair of nearly parallel filaments of emission which delineate the walls of a 0.1 pc wide cavity. The filaments converge to pinch the cavity about $17'$ west of IRS 5 at the location of a relatively high velocity and bright knot of CO (L1551 W; Pound & Bally 1991). There is no known cloud core or IRAS source at this location. The E–W flow continues west of this knot as a narrow and fading CO filament right to the boundary of the mapped region. Visual wavelength and near-infrared imaging have failed to reveal any emission line objects associated with the E–W outflow lobe.

Figure 15 compares the $850\text{ }\mu\text{m}$, CO outflows, and optical emission from the cloud. There is no sign of HH objects, etc., within the outflow, or (especially) toward the high-velocity peak $20'\text{west}$ of IRS5. Unfortunately the $850\text{ }\mu\text{m}$ image doesn’t extend far enough west to tell if there is a continuum source at that position. Thus our data do not resolve the origin of this outflow.

3.3. L1551-MC

In figure 4, a dark, heavily extinguished bar can be seen extending $\sim 16'$ north-west of IRS5. About half way along this bar lies a lone Herbig-Haro object, HH 265, whose origin

is unknown. We have detected 850 μm emission associated with this dark bar, in the neighborhood of HH 265. The emission (Fig. 1) appears as a roughly elliptical, weakly centrally condensed core, with peak intensity $\sim 0.2 \text{ Jy beam}^{-1}$, and integrated intensity $\sim 4.5 \text{ Jy}$ at 850 μm .

The 850 μm continuum emission coincides with an NH_3 clump discovered by Swift, Welch & Di Francesco (2005) (Figure 16), which they've dubbed L1551-MC. Their NH_3 core is roughly of size $2.5' \times 1.11'$ ($0.110 \times 0.054 \text{ pc}$ at 168 pc distance) aligned with the orientation of the dark bar, and has an average density of $10^4\text{-}10^5 \text{ cm}^{-3}$, kinetic temperature of $T_K \sim 9\text{K}$, and total mass of $\sim 2M_\odot$ (Swift, Welch & Di Francesco 2005). If we, too, assume a dust temperature of 9K, then we derive a mass of the clump of $2.6 M_\odot$, which is very similar to their value. (Using $T_d=20\text{K}$ gives $0.6 M_\odot$ (Table 1).)

The column density of dust emission peaks at the same location as NH_3 emission peaks (Figure 16). Swift, Welch & Di Francesco (2005) found that CCS emission, conversely, was depleted toward the column density peak. They found no evidence for an embedded protostar, but did find that the kinematics of the CCS emission suggests that the outer regions, at least, of the core are undergoing infall.

If this core is indeed infalling and eventually collapses, will this core form an isolated protostar or fragment into a small cluster of stars similar to the HL/XZ Tau group? The total mass still within the HL/XZ Tau core is of order $1 M_\odot$ or so, although we are likely to have missed some emission because of chopping. The mass of stars is also of order $1\text{-}2 M_\odot$, so roughly 50% of the mass has gone into protostars. If the L1551-MC core is similar, then $\sim 1 M_\odot$ will form into protostars, enough mass to form several low-mass stars.

There is no evidence from the NH_3 data (Figure 16, magenta contours) that the clump has begun to fragment, at least at the $\sim 30''$ resolution of the observations. The $\sim 14''$ resolution 850 μm data is lumpier, but the “lumpiness” is of the same order as the variance in this part of the image, and thus shows no evidence for fragmentation of the clump.

3.4. Origin of HH 265

The HH object HH 265 lies on the south-eastern end of the L1551-MC core (Figure 16). It is unlikely that the origin of this object lies within the clump, since the clump appears to be prestellar. Furthermore the morphology of the HH object is that of a working surface ahead of a bow shock (Figure 16), with orientation of the complex extending north-eastward toward the HL Tauri group (Fig. 7). Furthermore, we see weak blue-shifted CO emission within the bow shock, extending still further north-east in the direction of the HL Tau group,

one member of which must therefore be the source of this HH object. None of the known jets (Figure 9), however, is oriented in the direction of HH 265, and all members of the group except LkHa358 are known to have jets. Thus LkHa358 is a likely candidate for the origin of this HH object, although it must be noted that a plume of emission associated with LkHa358 (Fig. 7) is oriented nearly due west, and not in the direction of HH 265. A line linking HH 265 with LkHa358 (shown in Fig. 17) passes very near to two faint H α emission knots at $4^h31^m19.8^s +18^\circ12'30.3''$ (knot A in Fig. 17) and $4^h31^m23.2^s +18^\circ12'54.5''$ (knot B). Extending this line further intersects another knot of H α emission at $4^h31^m49.4^s +18^\circ14'50.7''$ (knot C). This line also comes very close to passing through HL Tau, and comes within only a few arcsec of XZ Tau. If these emission features are related, it would indicate a new, previously unknown jet originating from LkHa358, or possibly from the binary companion of XZ Tau, or a currently unknown binary companion of HL Tau.

4. Discussion and Summary

In this paper, we present new sub-millimeter dust continuum maps and J=2-1 CO images of the L1551 cloud in the Taurus cloud complex. These data are combined with deep visual wavelength images and analyzed in the context of the extensive literature on this nearby star forming cloud.

All previously known Class 0 and Class I YSOs in L1551 are detected in the 850 μ m sub-mm continuum images. Furthermore, no new compact sub-mm sources were found. Thus, the inventory of highly embedded young stellar objects appears to be complete. However, it is possible that the known Class 0/I protostars contain additional members which remain unresolved in our data.

The compact sub-mm emitters are concentrated in two sub-clusters. The binary system IRS5, the most luminous and massive YSO in L1551, and the L1551-NE multiple system, are located near the southeastern end of the cloud. Both members of IRS5 and one member of the NE system power nearly parallel jets which appear to be collectively responsible for powering the main CO outflow in this cloud. While the IRS5 binary and its HH 154 jet clearly power HH 102 and the northern rim of the CO outflow complex, NE is responsible for the highly collimated HH 454 jet and [SII] knots, the bright HH object HH 29, possibly HH 28, the eastern portion of HH 262, and possibly the distant bow shock HH 286. Thus, one member of the NE system is responsible for the southern portion of the main CO outflow lobes.

The driving source of the large redshifted east-west CO lobe originating near HH 102

remains unclear. Our SCUBA observations did not find any additional YSO candidates along the axis of this outflow lobe. However, the orientation of this limb-brightened low-velocity outflow lobe suggests that the driving source may one member of the L1551-NE multiple star syst.

The second sub-cluster of sub-mm emitters consists of the sources clustered around HL Tau (HH 30*, XZ Tau, and LkH α 358). All four of these YSOs are associated with 850 μ m emission with HL Tau being by far the brightest. LkH α 358 (or perhaps the binary companion of XZ Tau or a currently unknown binary companion of HL Tau) may be the origin of a jet terminating at HH 265. A very weak molecular outflow was detected associated with the end of this jet.

In addition to the compact sources, the sub-mm continuum emission exhibits diffuse components. Ridges of 850 μ m emission extends from IRS5 to HH 102, from IRS5 towards the axis of the southwestern CO lobe, from IRS5 towards NE, and from NE towards HH 262. The brightest parts of both HH 102 and HH 262 are detected at 850 μ m. Although CO J = 3-2 emission may make a small contribution to this emission, most of the flux is likely to be produced by warm dust entrained by outflows. A complex halo of dust emission also surrounds the HL Tau region. This extended emission may compromise the use of this YSO as a secondary calibrator for sub-mm continuum observations.

The L1551 cloud is cometary, indicating progressive erosion from the general direction of Orion, located to the southeast. Deep wide-field visual wavelength images and CO maps show that the L1551 cloud has a cometary morphology consisting of a dense head near the IRS5 / NE and HL Tau region, and a diffuse tail extending more than a degree towards the northwest. The densest part of this diffuse tail can be clearly seen in our [SII] image (Figure 4). Diffuse 850 μ m dust emission is produced by this region, dubbed L1551-MC. This object is likely to be a pre-stellar core showing signs of undergoing the first phases of gravitational collapse (Swift, Welch, & Di Francesco 2005). We do not see any signs of fragmentation of the clump. Assuming a dust temperature of 9 K, our sub-mm continuum flux implies a total mass of order 3 M_{\odot} .

The wide-field [SII] image (Figure 4) shows that the southeastern rim of the L1551 cloud is illuminated from the southeast. The CO maps show that the cloud has a sharp edge in this direction. Many background galaxies are visible beyond the southeastern edge of the cloud, indicating that this portion of the cloud has been dispersed. The locations of the older Class II and Class III YSOs born from the L1551 cloud indicate that stars formed relatively recently southeast of the current cloud edge (Figure 4). The cometary shape of the L1551 cloud, the projected distribution of older YSOs, the faint glow along the southeastern rim of L1551, and the location of L1551-MC northwest of the recently formed Class 0/I YSOs

indicate that the L1551 cloud has been irradiated and eroded from the general direction of Orion.

The currently active sites of star formation in Orion are located between 380 and 470 pc from the Sun. However, the older sub-groups of the Orion OB association are located closer with some members of the 1a and 1b subgroup as near as 300 pc, about 150 pc from L1551 (de Zeeuw et al 1999). The closest portion of the Orion-Eridanus supershell, the H α feature known as the Eridanus Loop (Reynolds, & Ogden 1979; Boumis et al. 2001), has been estimated to be only 160 pc from the Sun (Burrows & Guo 1996), which places it within 50 pc of L1551. Portions of the 21 cm HI supershell driven by the Orion OB association and 100 μ m dust emission traced by the IRAS satellite are located well outside the H α loops illuminated by Orion's massive stars (e.g. Brown, Hartnamm, & Burton 1995; Heiles, Haffner, & Reynolds 1999).

The two well-known massive stars, Betelgeuse and Rigel, are located in the closer-parts of the Orion-Eridanus supershell and southeast of L1551. Betelgeuse, is about 130 pc from the Sun and has an 18 km s $^{-1}$ proper motion towards PA $\sim 68^\circ$. Rigel is located 240 pc from the Sun and illuminates a small complex of star-forming molecular clouds associated with IC 2118 in the southwester portion of Orion (Kun et al. 2004). The proper motion of Betelgeuse (7.6 milliarcsec /year) would place it southeast of L1551 several million years ago. Thus, both of these massive stars could have been within 100 pc of the L1551 cloud within the last several million years and may have contributed to the photo-erosion of this cloud.

In summary, distribution of YSOs, the cometary shape, the external illumination, and location of the pre-stellar core L1551-MC indicate that the evolution of the L1551 cloud has been influenced by massive stars and photo-erosion from the general direction of Orion. The closest parts of the Orion OB associations, and massive stars in the direction of Orion may be responsible for the evolution of the L1551 cloud.

The research of D.J. is supported through a grant from the Natural Sciences and Engineering Research Council of Canada. Thanks to Youssef Billawala for supplying the reduced CO J=2-1 map of the region and to Jonathon Swift for supplying the molecular line maps of L1551-MC. The JCMT is operated by the Joint Astronomy Centre on behalf of the Particle Physics and Astronomy Research Council of the UK, the Netherlands Organization for Scientific Research, and the National Research Council of Canada. The authors acknowledge the data analysis facilities provided by the Starlink Project which is run by CCLRC on behalf of PPARC. Data mining was done using facilities of the Canadian Astronomy Data Centre, which is operated by the Dominion Astrophysical Observatory for the National Research

Council of Canada’s Herzberg Institute of Astrophysics.

REFERENCES

Bertout, C., Robichon, N., & Arenou, R. 1999, A&A, 352, 574

Boumis, P., Dickinson, C., Meaburn, J., Goudis, C. D., Christopoulou, P. E., Lopez, J. A., Bryce, M., & Redman, M. P. 2001, MNRAS 320, 61

Briceño, C., Hartmann, L., Stauffer, J., & Martín, E. 1998, AJ, 115, 2074

Briceño, C., Stauffer, J. R., & Kirkpatrick, J. D. 2002, ApJ, 580, 317

Brown, A., Drake, S. A., & Mundt, R. 1985, in *Radio Stars*, ed. R. M. Hjellming and D. M. Gibson (Dordrecht: Reidel), p.105

Brown, A. G. A., Hartmann, D., & Burton, W. B. 1995, \AA , 300, 903

urrows & Guo 1996

Carkner, L., Feigelson, E. D., Koyama, K., Montmerle, T., & Reid, I. N. 1996, ApJ, 464, 286

Chandler, C. J., & Richer, J. S. 2000, ApJ, 530, 851

Cudworth, K. M., & Herbig, G. 1979, AJ, 84, 548

Devine, D., Reipurth, B., & Bally, J. 1999, AJ, 118, 972

Devine, D., Reipurth, B., & Bally, J. 2000, ApJ, 540, L57

de Zeeuw, P. T., Hoogerwerf, R., de Bruijne, J. H. J., Brown, A. G. A., & Blaauw, A. 1999, AJ, 117, 354

Emerson, J. P., Harris, S., Jennings, R. E., Beichman, C. A., Baud, B., Beintema, D. A., Wesselius, P. R., & Marsden, P. L. 1984, ApJ, 278, L49

Favata, F., Giardino, G., Micela, G., Sciortino, S., & Damiani, F. 2003, A&A, 403, 187

Feigelson, E. D., & DeCampli, W. M. 1981, ApJ, 243, L89

Feigelson, E. D., & Kriss, G. A. 1983, AJ, 88, 431

Feigelson, E. D., Jackson, J. M., Mathieu, R. D., Myers, P. C., & Walter, F. M. 1987, AJ, 94, 1251

Fridlund, M. & Liseau, R. 1998, ApJ, 499, L75

Gålfalk, M., *et al.* 2004, A&A, 420, 945

Gomez, M., Jones, B. F., Hartmann, L., Kenyon, S. J., Stauffer, J. R., Hewett, R., & Reid, I. N. 1992, ApJ, 104, 762

Graham, J. A. & Heyer, M. H. 1990, PASP, 102, 972

Hartigan, P., Morse, J., Palunas, P., Bally, J., & Devine, D. 2000, AJ, 119, 1872

Heiles, C., Haffner, L. M., & Reynolds, R. J. 1999 in Taylor A. R., Landecker, T. L., Joncas, G. eds. ASP Conf.Ser.Vol. 168, New Perspectives on the Interstellar Medium, Astron.Soc.Pac., San Francisco

Herbig, G. 1974, Lick Obs. Bull, No. 658

Holland, W. S., *et al.* 1999, MNRAS, 303, 659

Jenness, T., *et al.* 2002, MNRAS, 336, 14

Johnstone, D., Wilson, C. D., Moriarty-Schieven, G., Giannakopoulou-Creighton, J., & Gregersen, E. 2000, ApJS, 131, 505

Johnstone, D., Boonman, A. M. S., & van Dishoeck, E. F. 2003, å, 412, 157

Jones, B. F., & Herbig, G. 1979, AJ, 84, 1872

Krist, J. E., *et al.* 1999, ApJ, 515, L35

Kun, M., Prusti, T., Nikolić, S., Johansson, L. E. B., & Walton, N. A. 2004, å, 418, 89

Looney, L. W., Mundy, L. G., & Welch, W. J., ApJ, 484, L157

López, R., Raga, A. C., Riera, A., Anglada, G., & Estalella, R. 1995, MNRAS, 274, L19

López, *et al.* 1998, AJ, 116, 854

Luyten, W. J. 1963, Harvard Annual Card No. 1589

Luyten, W. J. 1971, The Hyades, Univ. Minnesota P., Minneapolis

Lynds, B. T. 1962, ApJS, 7, 1

Mangum, J. 1997, NRAO Publication: *On The Fly Observing at the 12m*

Monin, J.-L., Pudritz, R. E., & Lazareff, B. 1996, *å*, 305, 572

Moriarty-Schieven, G. H., Butner, H. M., & Wannier, P. G. 1995, *ApJ*, 445, L55

Moriarty-Schieven, G. H., & Snell, R. L. 1988, *ApJ*, 332, 364

Moriarty-Schieven, G. H., Snell, R. L., Strom, S. E., & Grasdalen, G. L. 1987, *ApJ*, 317, L95

Moriarty-Schieven, G. H., Powers, J. A., Butner, H. M., Wannier, P. G., & Keene, J. 2000, *ApJ*, 533, L143

Moriarty-Schieven, G. H. & Wannier, P. G. 1991, *ApJ*, 373, L23

Mundt, R., Brugel, E. W. & Bührke, T. 1987, *ApJ*, 319, 275

Mundt, R., Bührke, T., & Ray, T. P. 1988, *ApJ*, 333, L69

Mundt, R., Bührke, T., Solf, J., Ray, T. P., & Raga, A. C. 1990, *å*, 232, 37

Onishi, T., Mizuno, A., Kawamura, A., Tachihara, K., & Fukui, Y. 2002, *ApJ*, 575, 950

Palla, F., & Stahler, S. W. 2002, *ApJ*, 581, 1194

Pound, M. W., & Bally, J. 1991, *ApJ*, 383, 705

Reynolds, R. J., & Ogden, P. M. 1979 *ApJ*, 229, 942

Riera, A., Raga, A., Lopez, R., Anglada, G. & Estalella, R. 1995, *Ap&SS*, 224, 551

Rodriguez, L. F., Roth, M., Canto, J., Tapia, M., Persi, P., & Ferrari-Toniolo, M. 1986, Rev. Mexicana Astron. Astrofis., 12, 285

Rodriguez, L. F., Anglada, G. & Raga, A. 1995, *ApJ*, 454, L149

Rodriguez, L. F., D'Alessio, P., Wilner, D. J., Ho, P. T. P., Torrelles, J. M., Curiel, S., Gomez, Y., Lizano, S., Pedlar, A., Canto, J., & Raga, A. C. 1998, *Nature*, 395, 355

Rodríguez, L. F., Curiel, S., Cantó, J., Loinard, L., Raga, A. C., & Torrelles, J. M. 2003a, *ApJ*, 583, 330

Rodríguez, L. F., Porras, A., Claussen, M. J., Curiel, S., Wilner, D. J., & Ho, P. T. P. 2003b, *ApJ*, 586, L137

Sandell, G., & Weintraub, D. A., 2001, *ApJS*, 134, 115

Sharpless, S. 1959, ApJS, 4, 257

Snell, R. L., Bally, J., Strom, S. E., & Strom, K. M. 1985, ApJ, 290, 587

Snell, R. L., Loren, R. B., & Plambeck, R. L. 1980, ApJ, 239, L17

Strom, S. E., Grasdalen, G. L., & Strom, K. M. 1974, ApJ, 191, 111

Swift, Jonathan J., Welch, William J., & Di Francesco, James. 2005, ApJ, in press (astro-ph/0411157)

Wood, K. S., *et al.* 1984, ApJS, 56, 507

Table 1. Submillimeter Continuum Properties of Sources in L1551

Source	Peak _{850μm} Jy beam ⁻¹	Integ _{850μm} Jy	^a Size _{850μm} arcsec	Peak _{450μm} Jy beam ⁻¹	Integ _{450μm} Jy	Size _{450μm} arcsec	Mass ^b M _⊕
<i>HL Tau Region</i>							
HL Tau	2.15	2.29	6.3×6.0	9.36	9.62	4.5×4.4	0.32
LkH α 358	0.05	<0.13	0.007
XZ Tau	0.01	<0.20	0.0014
HH 30*	0.05	<0.13	0.007
Plateau	0.05	5.23	80.7×51.8				0.73
<i>L1551 Region</i>							
IRS5	3.16	7.23	10.2×8.0	17.4	45.7	8.1×6.2	1.01
NE	1.16	2.78	9.8×8.8	5.7	8.33	7.4×6.9	0.39
Plateau	0.18	19.05	99.0×40.5				2.67
North-east Lobe		~0.2			~2.9		0.03
South-west Lobe		~0.3			...		0.04
<i>L1551-MC/ Dark Arc</i>							
L1551-MC	0.05	4.5	100×33.2				0.63
Embedded Source	0.04	0.2	16.1×12.0				0.028

^aDeconvolved sizes.

^bMass derived from the total flux at 850 μ m assuming $T_d = 20$ K and $\kappa_{850} = 0.02$ cm²g⁻¹.

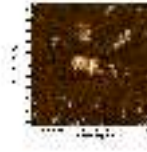


Fig. 1.— $850\mu\text{m}$ image of the L1551 molecular cloud revealing the HL Tau region (north), the IRS 5/NE region (center), the L1551 outflows, (left and right), and the L1551-MC region (upper right). Contour intervals are at 0.035, 0.07, 0.14, 0.28, 0.56, 1.12 and $2.24 \text{ Jy beam}^{-1}$.

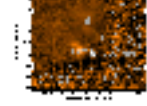


Fig. 2.— $450\mu\text{m}$ image of L1551 molecular cloud toward HL Tau and IRS5/NE. Contour intervals are at 0.15, 0.3, 0.6, 1.2, 2.4 and 4.8 Jy beam^{-1} .

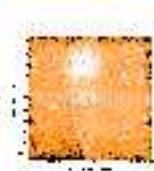


Fig. 3.— RMS variance for the $850\mu\text{m}$ image. Note that the uncertainty is much less in regions where multiple measurements have been obtained, primarily toward the HL Tau region, where the variance reaches a minimum of $0.0017 \text{ Jy beam}^{-1}$. The white contour is at $0.010 \text{ Jy beam}^{-1}$, black contours are at $0.012, 0.014$ and $0.016 \text{ Jy beam}^{-1}$, and grey contours run from 0.008 to $0.002 \text{ Jy beam}^{-1}$ at intervals of $0.002 \text{ Jy beam}^{-1}$. Apparent variance peaks toward IRS5, NE and HL Tau are artifacts of the reconstruction process.

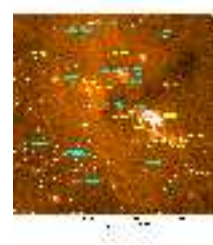


Fig. 4.— [SII] image of L1551 cloud. Known PMS and YSOs are labeled along with selected Herbig-Haro objects. Note the dark arc to the north-west of IRS5.

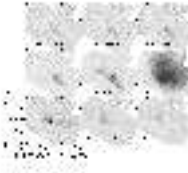


Fig. 5.— Channel maps of CO J=2-1 emission.

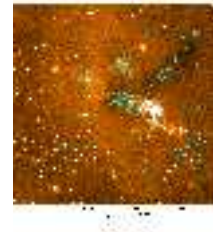


Fig. 6.— [SII] image with contours of $850\mu\text{m}$ emission overlaid. Contour intervals same as in Figure 1.

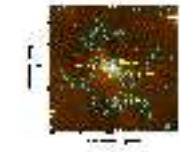


Fig. 7.— Same as Figure 6, but focusing on the HL Tau group. Contours are 0.015, 0.03, 0.06, 0.12, 0.24, 0.48, 0.96, and $1.92 \text{ Jy beam}^{-1}$.

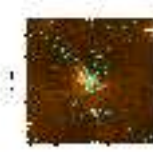


Fig. 8.— [SII] image of the HL Tau region with $450\mu\text{m}$ emission contours overlaid. Contour levels are 0.1, 0.2, 0.4, 0.8, 1.6 and 3.2 Jy beam^{-1} . The “+” marks the location of the proposed source VLA1 (Mundt, Brugel & Bührke 1987).



Fig. 9.— HL/XZ Tau outflow in $^{12}\text{CO}_{2-1}$. The blue lobe (solid contours) is velocity integrated from 1.0 km s^{-1} to 6.0 km s^{-1} . The red lobe (dotted contours) is velocity integrated from 9.0 km s^{-1} to 14 km s^{-1} . Contour levels = 3, 4, 5, ... K km s^{-1} .

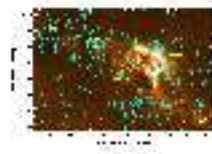


Fig. 10.— Same as Figure 6, but focusing on the IRS5/NE outflow. Contours are 0.02, 0.04, 0.08, 0.16, 0.32, 0.64, 1.28, and 2.56 Jy beam^{-1} .

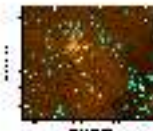


Fig. 11.— Same as Fig. 6, but focusing on the region to the north-east of L1551 NE. Contours same as Figure 10.

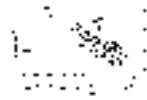


Fig. 12.— The main L1551 outflow in $^{12}\text{CO}_{2-1}$. The southwest lobe (solid contours) is velocity integrated from -6.0 km s^{-1} to 6.0 km s^{-1} . The NE lobe (dotted contours) is velocity integrated from 7.0 km s^{-1} to 20.0 km s^{-1} . Contour levels = 16, 20, 24, ... K km s^{-1} .

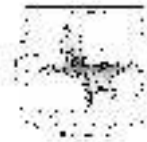


Fig. 13.— $^{12}\text{CO}_{2-1}$ velocity slice through HH 262, IRS 5, and HH 28. Contours are for 0.4, 1.4, 2.4, ... K km s^{-1} .



Fig. 14.— Contours of $850 \mu\text{m}$ emission overlaid on a grey-scale image of the blue-shifted CO emission ($4-6 \text{ km s}^{-1}$) (above), and red-shifted CO emission ($10-12 \text{ km s}^{-1}$) (below). Contour intervals the same as in Figure 1.

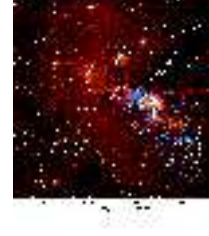


Fig. 15.— Comparison of the $850\mu\text{m}$ emission (white contours, same intervals as Fig. 1), CO outflows (red-shifted ($8\text{-}10\text{ km s}^{-1}$) and blue-shifted ($4\text{-}6\text{ km s}^{-1}$) emission as red and blue contours respectively (intervals at $2, 4, 6, \dots \text{ K km s}^{-1}$)),, ambient CO emission (orange contour at 2 K km s^{-1}), and optical [SII] emission (greyscale) from the L1551 cloud.

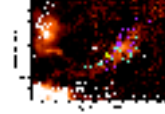


Fig. 16.— $850\mu\text{m}$ dust continuum image in greyscale, with overlaid with contours of NH_3 (magenta, contours at intervals of $0.5, 1, 1.5, \dots \text{ K km s}^{-1}$), CCS (cyan, intervals $0.05, 0.1, 0.15, \dots \text{ K km s}^{-1}$), CO $J=2\text{-}1$ wing emission (white, contours $1.25, 1.75, 2.25, \dots \text{ K km s}^{-1}$), integrated over $4\text{-}6\text{ km s}^{-1}$, and [SII], in yellow, indicating the position and morphology of HH 265.

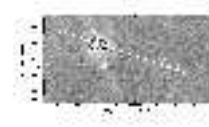


Fig. 17.— Greyscale of the difference image between $\text{H}\alpha$ and [SII] toward the HL Tau region, and showing the orientation of a possible jet from LkH α 358 or HL Tau, culminating at HH 265 The greyscale is “wrapped” to display subtle features. Knots along the suggested jet toward HH 265 are indicated as a, b, and c.